Journal of Alloys and Compounds 509 (2011) 8360–8364

Contents lists available at ScienceDirect

Journal of Alloys and Compounds

journal homepage: www.elsevier.com/locate/jallcom

$Ce_{0.9}Sr_{0.1}Cr_{0.5}Fe_{0.5}O_{3-\delta}$ as the anode materials for solid oxide fuel cells running on H_2 and H_2S

Xiufang Zhu[a], Han Yan[a], Qin Zhong[a,*], Xuejun Zhao[a], Wenyi Tan[a,b]

[a] School of Chemical Engineering, Nanjing University of Science and Technology, Nanjing 210094, PR China
[b] Department of Environment Engineering, Nanjing Institute of Technology, Nanjing 211167, PR China

ARTICLE INFO

Article history:
Received 4 January 2011
Received in revised form 18 March 2011
Accepted 19 March 2011
Available online 29 March 2011

Keywords:
Solid oxygen fuel cell
Anode catalyst
Perovskite structure
Electrical conductivity
H_2S

ABSTRACT

$Ce_{0.9}Sr_{0.1}Cr_{0.5}Fe_{0.5}O_{3-\delta}$ (CSCrF) powders were synthesized by gel combustion method and the conductivities have been evaluated with DC four-probe method in 3% H_2–N_2 and 5% H_2S–N_2 at 400–800 °C, respectively. XRD shows that CSCrF powders have cubic perovskite structure which is similar to that of $CeCrO_3$ (JCPDS card No. 75-0289). Meanwhile, CSCrF exhibits good chemical compatibility with electrolyte ($Ce_{0.8}Sm_{0.2}O_{1.9}$) in N_2. Through analysis of XRD and IR, some $Ce_{0.9}Sr_{0.1}Cr_{0.5}Fe_{0.5}(O, S)_{3-\delta}$ are produced after exposure to 5% H_2S–N_2 at 800 °C for 5 h, which has a resemblance to Refs. [1,2]. The electrochemical properties were measured for the cell comprising CSCrF–$Sm_{0.2}Ce_{0.8}O_{1.9}$/$Sm_{0.2}Ce_{0.8}O_{1.9}$/Ag in 5% H_2S at low temperature (450, 500, 550 and 600 °C), and in 3% H_2–N_2 at 500 °C, respectively. Electrochemical impedance spectroscopy (EIS) and the equivalent circuit reveal that polarization resistance is the main reason affecting the performance of the cell at low temperature. The area specific resistance significantly decreases with the increasing temperature.

1. Introduction

Each year over 40×10^6 tons of hydrogen sulfide is produced worldwide, mostly as by-products from heavy oil desulfurization processes, natural gas industry and coal gasification/liquefaction [3,4]. For the adverse effects of H_2S on environment, equipment and human health, disposal and treatment of it from every effluent is regarded as a worldwide problem. The typical methods to remove H_2S include Claus process [5] and Tannin extract process [6]. However, these reactions are highly exothermic. During H_2S disposal process, only part of the energy can be recovered as low-grade energy during the steam produced, while other is wasted. In 1987, Pujare et al. [7] first proposed the H_2S/air solid oxide fuel cell to remove H_2S. Due to toxicity of H_2S to anode, searching for suitable anodes is of vital importance. In the last 30 years, many groups had tried to find anodes materials for SOFC operated on H_2S, such as various thiospinel (CrV_2S_4 [8], MoV_2S_4 [9,10], and $CoMo_2S_4$ [11], etc.), metal sulfide (MoS_2 [12,13], WS_2 [14], and NiS_2–MoS_2, etc. [15–18]), and perovskite structure ($La_xSr_{1-x}VO_{3-\delta}$ [19–23]). The performances of them exhibit good tolerance to H_2S and high electrochemical properties.

In 2009, Luo et al. performed studies on $Ce_{0.9}Sr_{0.1}Cr_{0.5}V_{0.5}O_3$ (CSCV) [1] and $Ce_{0.9}Sr_{0.1}VO_3$ [2], the results revealed that these anode materials had higher activity for conversion of H_2S than CH_4. $Ce^{3+/4+}$ maybe can provide a secondary active site (besides $V^{3+/4+/5+}$) on the surface of the anode, and several Ce based perovskites as anodes were listed in a Japanese patent [24]. However, for V-base compounds poisonous to health and the higher cost, in this work, Fe-base compounds as nontoxic and cheaper materials are chosen to replace V-based compounds.

The performances of $Ce_{0.9}Sr_{0.1}Cr_{0.5}Fe_{0.5}O_{3-\delta}$ powders as anode material in SOFC fuelled with H_2S and H_2 are characterized at low temperature. The morphology and the crystal structure of the synthesized powders are examined. Additionally, the conductivity and the electrochemical property are measured at various temperatures and atmospheres.

2. Experimental

2.1. Preparation of anode materials

$Ce_{0.9}Sr_{0.1}Cr_{0.5}Fe_{0.5}O_{3-\delta}$ (CSCrF) powders were synthesized by gel combustion method [1]. The prepared process was described as follows. Stoichiometric $Ce(NO_3)_3{\cdot}6H_2O$, $Sr(NO_3)_2$, $Cr(NO_3)_3{\cdot}9H_2O$ and $Fe(NO_3)_3{\cdot}9H_2O$ were weighed and dissolved in distilled water. Citric acid was added with stirring. Ammonium hydroxide was applied to adjust the pH to ~7. Under stirring and heating, a viscous gel was obtained, which was heated continually until combusted to get porous ash. The ash was calcined in air at 900 °C for 2 h. Finally, the powders were reduced in 3% H_2–N_2 at 1100 °C for 5 h.

2.2. Electrolyte and cathode

$Ce_{0.8}Sm_{0.2}O_{1.9}$ (SDC) powders as the electrolyte were prepared by EDTA–citric complexing method [25]. Sm_2O_3 pre-dissolve in HNO_3 and $Ce(NO_3)_3{\cdot}6H_2O$ were dis-

* Corresponding author. Tel.: +86 25 84315517; fax: +86 25 84315517.
E-mail addresses: zq304@mail.njust.edu.cn, xiufangzhu@163.com (Q. Zhong).

0925-8388/$ – see front matter © 2011 Elsevier B.V. All rights reserved.
doi:10.1016/j.jallcom.2011.03.124

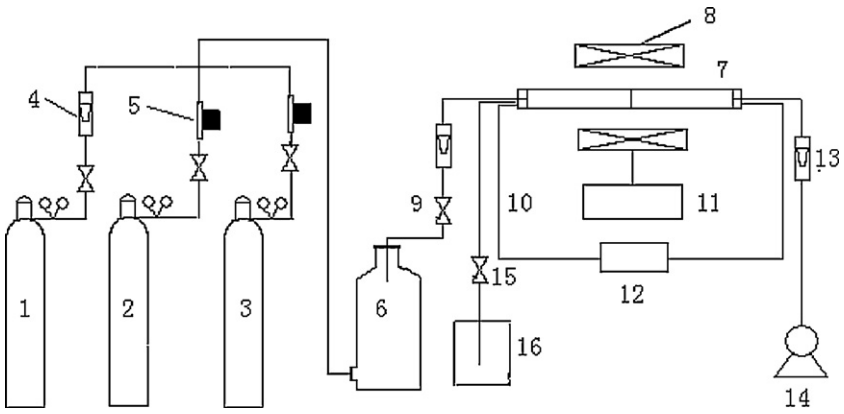

Fig. 1. Schematic diagram of experimental apparatus for sulfur-tolerant anode test. 1, $H_2S + N_2$ gas cylinder; 2, H_2 gas cylinder; 3, N_2 gas cylinder; 4, rotameter; 5, mass flow meter; 6, buffered bottle; 7, reactor of SOFC; 8, furnace; 9, intake port collection; 10, Au line; 11, temperature controller; 12, CHI660D electrochemical workstation; 13, air rotameter; 14, air compressor; 15, outtake port collection; and 16, off-gas absorption container.

solved at the stoichiometric ratio. A certain amount of EDTA–$NH_3 \cdot H_2O$ was dropped into it, and citric acid was added with stirring. Ammonia was used to adjust the pH to ~10. The solution was heated with stirring at above 90 °C to get a transparent gel. And then the gel was baked in 180 °C for 18 h. The powders were calcined at 900 °C for 6 h in air, and then pressed the powders into a pellet, the pellet's thickness is 0.8 mm and its diameter is 30 mm. The wafer was sintered at 1100 °C for 4 h as support.

The cathode material was silver epoxy adhesive (CB-813, CRCBonD Co, LTD). The cathode with the thickness of 50 μm was applied to electrolyte by the screen printing method. Then the sample was fired in N_2 at 800 °C for 4 h to achieve densification. As shown in Fig. 1 [26].

2.3. Characterization and electrochemical test

The precursor powders were characterized by XRD (Bruker D8 ADVANCE, Germany) with Cu Kα radiation in the range from 20° to 80°. The morphology of the precursor powders was measured through scanning electron microscopy (SEM) (Flexscan L367 S-3000N, HITACHI).

2.4. Conductivity testing

The anode powders were pressed into pellets and silver epoxy adhesive was pasted on both faces of the wafers. Conductivity measurements were carried out by the symmetrical cells in 3% H_2–N_2 and 5% H_2S–N_2 by 4-probe DC, respectively.

2.5. Chemical stability

Interfacial phase reaction between anode and electrolyte may incur some practical problems. For example, the non-conductive phases formed between electrolyte and electrode significantly increased the interfacial polarization resistance. To get more information about phase reaction between CSCrF and SDC, the chemical compatibilities of them were examined by heat-treating. The process was as follows, 50 wt% CSCrF and 50 wt% SDC were mixed, pressed into pellet, fired at 900 °C for 5 h in N_2. After cooling, the pellets were ground with a mortar and pestle. The phase composition of the powders was determined by XRD.

After exposure in 5% H_2S–N_2 at 800 °C for 5 h, the phase composition of the powders was evaluated by XRD and FT-IR.

2.6. Cell preparation

The Membranes were prepared by painting silver paste onto the electrolyte SDC to form the cathode. In order to increase the thermal compatibility with electrolyte and reduce the interface resistance, the anode catalysts CSCrF and SDC (4:1 by weight) were ground and dispersed in α-terpineol to form a viscous paste, and the paste was screen printed onto the opposite face of the electrolyte to form membrane electrode assemblies (MEAs). The MEAs (cell with configuration: anode/electrolyte/cathode: CSCrF–SDC/SDC/Ag) were pre-sintered at 800 °C in N_2 for 4 h. Au mesh was used as current collector to adhere to two surfaces of electrodes with Pt paste, and anode was fed with 5% H_2S and 3% H_2, respectively, while cathode with air.

The anode polarization resistance (R_p) and Ohm resistance (R_o) were measured via electrochemical impedance spectrum measurement by an electrochemical workstation (CHI660D, Chenhua, Shanghai). The range of the frequency was from 0.1 Hz to 10^6 Hz.

Electrolyte SDC is sensitive to react with reduction gases [31–34]. Roman spectrum is used to analyze the stability of SDC which utilizes in the cell test.

3. Results and discussion

3.1. XRD of precursor powders

The XRD pattern of the $Ce_{0.9}Sr_{0.1}Cr_{0.5}Fe_{0.5}O_{3-\delta}$ powders (Fig. 2) shows that the phase formations of the powder samples possess perovskite structures with. A cubic structure is observed with lattice parameters $a = 3.87$ Å. Similar to that of the $CeCrO_3$ parent (JCPDS card No. 75-0289) and the parameter is $a = 3.89$ Å. The average crystallite size is calculated using the Scherer's formula (1).

$$D = \frac{K\lambda}{\beta \cos \theta} \quad (1)$$

where D is average crystallite size, K is the Scherrer constant, λ is the wavelength of Cu-Kα radiation, θ is the Bragg diffraction angle, and β is the full width at half maxima (FWHM) of the diffraction peak. After correction the formula as followed (2):

$$D = \frac{0.89 \times 0.15406}{\frac{\beta - 0.09}{180} \times \pi \times \cos \theta} \quad (2)$$

The CSCrF prepared in 3% H_2 at 1100 °C has an average crystalline size of ~35 nm.

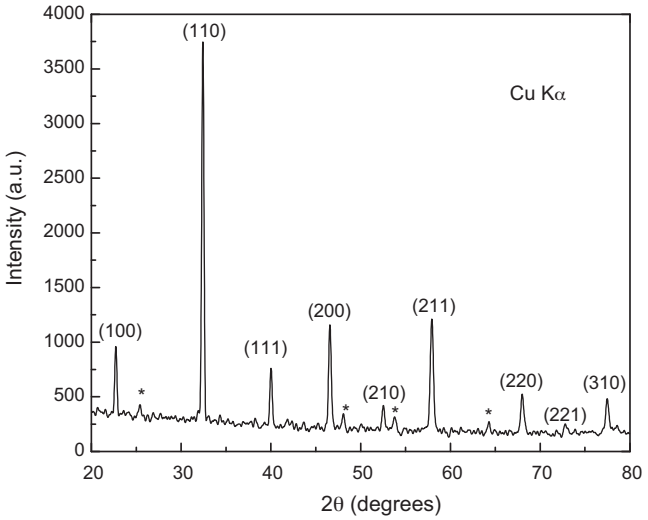

Fig. 2. XRD pattern of CSCrF powders after reduction in 3% H_2–N_2 at 1100 °C for 5 h.

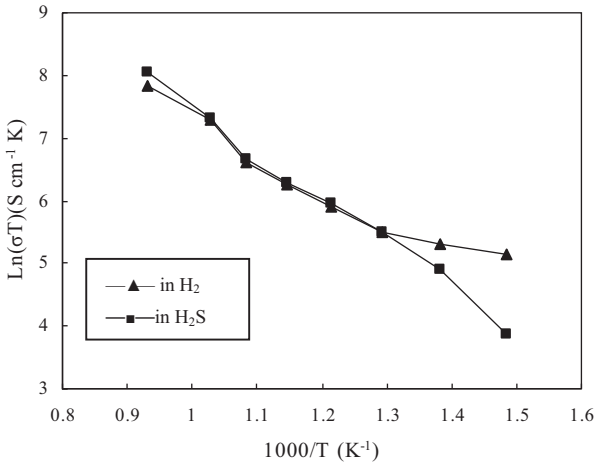

Fig. 3. Conductivities of CSCrF in 5% H_2S–N_2 and 3% H_2–N_2.

3.2. Conductivity testing

The conductivities of CSCrF were investigated in 3% H_2–N_2 and 5% H_2S–N_2. They increase with the temperature elevated as given in Fig. 3, behavior typical of semiconductors and ionic conductors [27]. The reason is mainly due to carrier (i.e. electron–hole) migration rate increasing with temperature. The highest conductivities are 2.92 S cm^{-1} in H_2S and 2.37 S cm^{-1} in H_2 at 800 °C. Fig. 3 illustrated that the conductivities in H_2 higher than in H_2S below 500 °C and after 500 °C they almost are equal, the reason maybe is H_2S beginning to decompose into H_2 at about 500 °C. The activation energies are 0.429 eV in H_2 and 0.614 eV in H_2S. The results indicate that CSCrF is favorable kinetically in H_2. Meanwhile, Fig. 3 indicates $\ln(\sigma T)$ with 1000 T^{-1} is a linear relationship which consistent with above Arrhenius equation (3) [28] at various temperatures.

$$\sigma = \left(\frac{C}{T}\right) \exp\left(\frac{-E_a}{kT}\right) \quad (3)$$

in which σ is the conductivity, E_a is the activation energy (eV); C is the pre-exponential term, T is the absolute temperature in Kelvin (K); $k = 0.86 \times 10^{-4}$ eV K^{-1} is the Boltzmann constant. After correction, equation is rewritten in a simple form

$$\ln(\sigma T) = \ln \quad C - \frac{E_a}{kT} \quad (4)$$

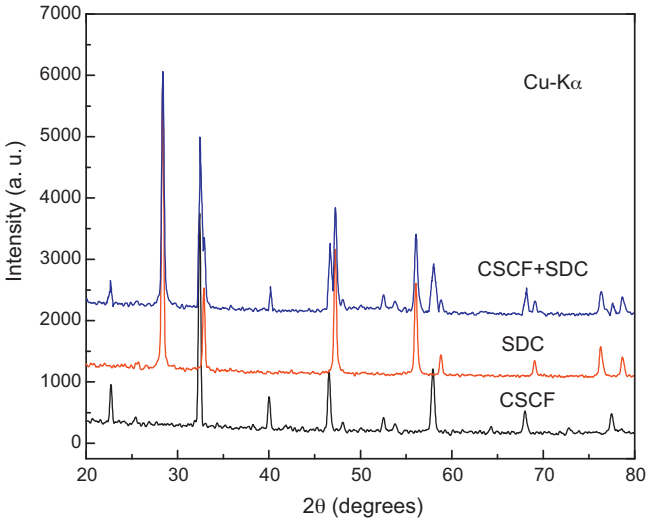

Fig. 4. XRD patterns of CSCrF, SDC and the mixture of them after calcined in N_2 at 900 °C for 4 h.

3.3. Chemical stability and powder morphology

Comparing the XRD patterns of CSCrF, SDC and the disc of CSCrF + SDC mixture after calcination in N_2 at 900 °C for 4 h, as shown in Fig. 4, it is clear that CSCrF has a good chemical compatibility with electrolyte SDC in N_2, and no other new phases are detected. The result shows $Ce_{0.9}Sr_{0.1}Cr_{0.5}Fe_{0.5}O_{3-\delta}$ is suitable to be used as the anode materials of electrolyte SDC. Comparing the XRD and IR of before and after exposure to H_2S at 800 °C for 5 h, some changes have happened as illustrated of CSCrF crystal structure in Fig. 5. The reason maybe is that some Ce–O–S phases are formed in so higher concentration H_2S. The result is consistent with that of CSCV and CSV [1,2].

Fig. 6 reveals the SEM micrographs of CSCrF after calcined in 3% H_2–N_2 at 1100 °C for 5 h. CSCrF catalyst particles are well dispersed and the structure has good porosity.

3.4. Electrochemical performance

Fuel cell tests are conducted to determine the electrochemical activity of the anode materials for conversion of H_2S, Figs. 7 and 8 show the I–V and I–P curves for CSCrF–SDC/SDC/Ag in 5% H_2S–N_2 at

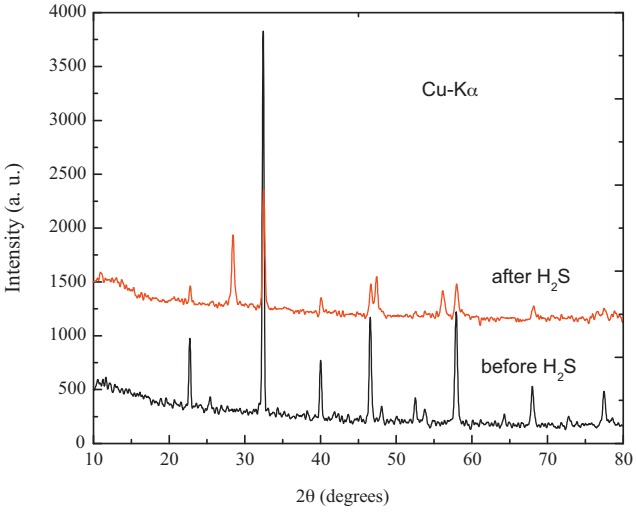

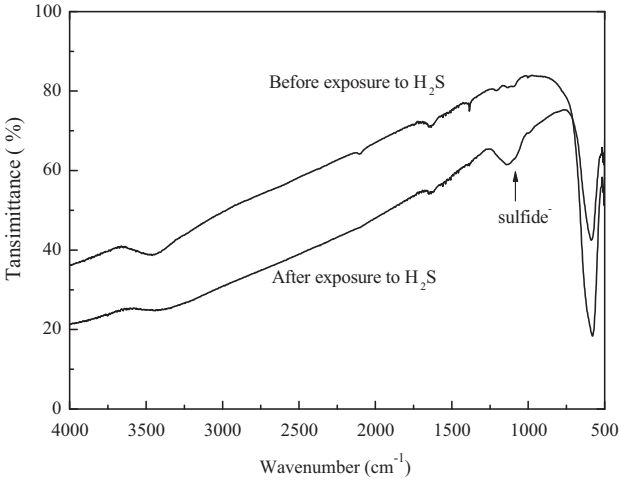

Fig. 5. XRD and IR patterns of CSCrF before and after exposure to 5% H_2S at 800 °C for 5 h.

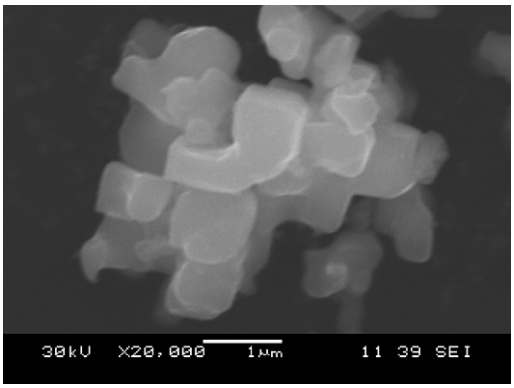

Fig. 6. SEM micrograph of CSCrF after calcined in 3% H_2–N_2 at 1100 °C for 5 h.

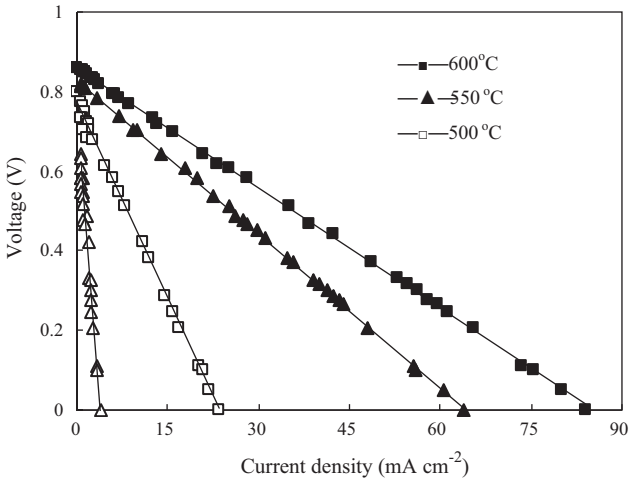

Fig. 7. *I–V* curves of single cell with CSCrF–SDC|SDC|Ag in 5% H_2S–N_2 at various temperatures.

various temperatures. The maximum open circuit voltage is 0.86 V and the maximum power density is 18.75 mW cm^{-2} at 600 °C. Fig. 9 indicates the *I–V* and *I–P* curves for the cell in 3% H_2–N_2 at 500 °C. The max OCV is 0.95 V and the max power density is 13.1 mW cm^{-2}. Comparing the max power density in H_2S to that of in H_2 at 500 °C, the power density is 4.1 mW cm^{-2} in H_2S while 13.1 mW cm^{-2} in H_2. The reason maybe is the toxity of H_2S to anode material and

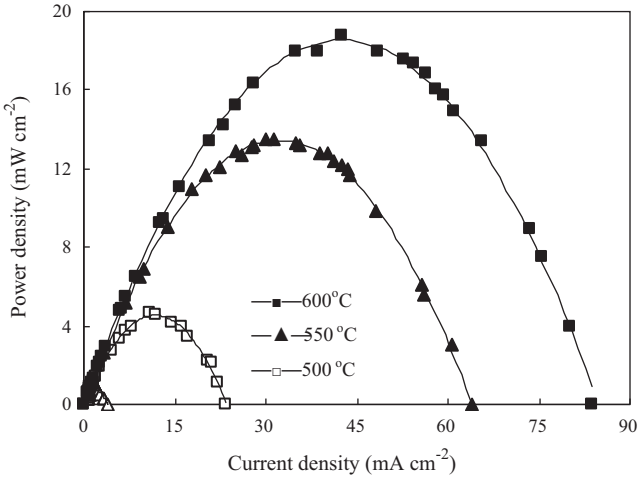

Fig. 8. *I–P* curves of single cell with CSCrF–SDC|SDC|Ag in 5% H_2S–N_2 at various temperatures.

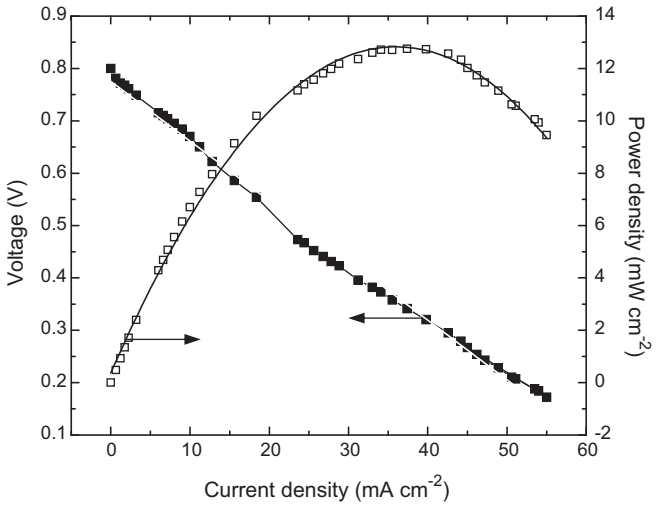

Fig. 9. *I–V* and *I–P* curves of single cell with CSCrF–SDC|SDC|Ag in 3% H_2–N_2 at 500 °C.

formation of Ce–S–O. The voltage with current density has the basic linear relationship, which indicates Ohm polarization is the main reason affecting the battery. Fig. 10 indicates that the OCV increase with rising of temperature in 3% H_2–N_2. The open-circuit voltage is sharply increasing after 470 °C for the migration of oxide-ionic being faster at high temperatures.

The interfacial impedance spectra for CSCrF in 3% H_2 at temperatures ranging from 400 to 500 °C are shown in Fig. 11, and the equivalent circuit for the analysis of the impedance data is illustrated in Fig. 12. Obviously, the area specific resistance significantly decreases with the increasing temperature as shown in Fig. 11. The impedance spectra consisted of two semi-circles. This means that there are at least two electrode processes corresponding to the two semi-circles during molecular hydrogen oxidation. According to Refs. [29,30], the semi-circle at the high frequency can be regarded as the polarization induced by charge transfer. On the other hand, the semi-circle at the low frequency can be considered to physical process which is anode gas adsorption/dissociation and bulk or surface hydrogen diffusion process. Therefore, in the equivalent circuit in Fig. 12, L1 is an inductance caused by the cables; R1 stands for the Ohmic resistance including the electrolyte resistance and lead wires [31]. R2 is represented as the resistance produced on the TPB; R3 is referred to the resistance of the anode gas (hydrogen)

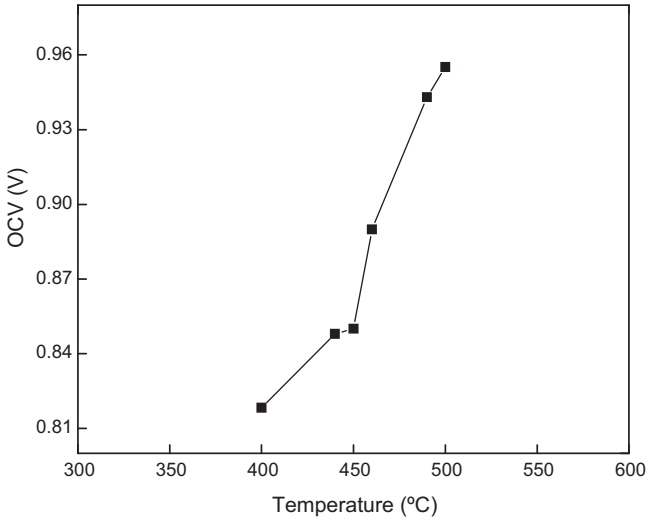

Fig. 10. OCV–*T* curve for CSCrF–SDC|SDC|Ag in 3% H_2–N_2.

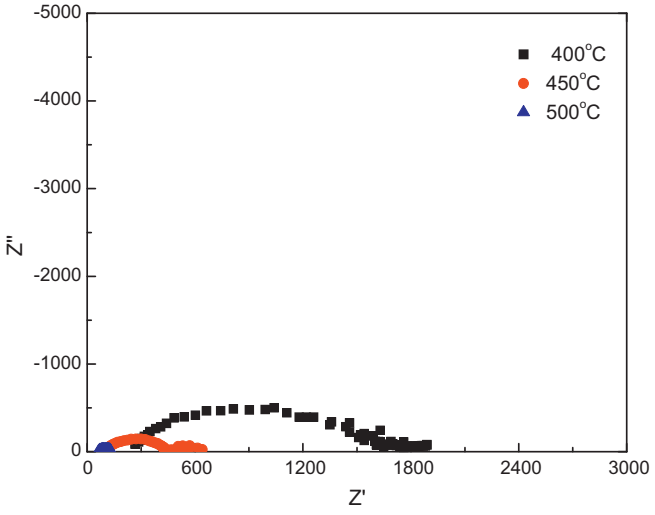

Fig. 11. EIS of CSCrF electrode at various temperatures.

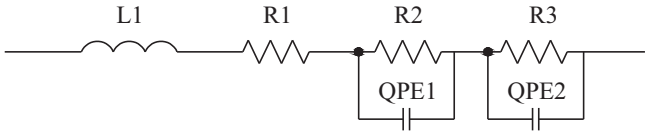

Fig. 12. Equivalent circuit model of EIS at 500 °C.

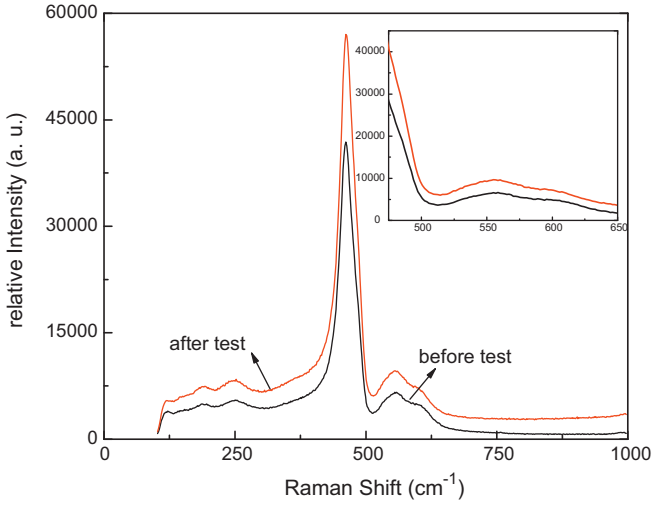

Fig. 13. Raman spectrums of SDC before and after cell test in 3% H_2.

adsorption/desorption and bulk or surface diffusion process; QPE1 and QPE2 correspond to the capacitance of the whole electrode.

After cell test, Raman spectrum of electrolyte SDC was given in Fig. 13. Comparing before and after test, a conclusion can be drawn that SDC is not reduction as electrolyte of the cell fuelled with H_2. An intense Raman band around 465 cm^{-1} is the Raman spectra of CeO_2, fluorite structure-metal dioxides have only a single allowed Raman mode, which has F_{2g} symmetry and can be viewed as a symmetric breathing mode of the O atoms around each cation [32–35]. In addition to the F_{2g} phonon mode, two low-intensity bands are detected at ~510 and ~630 cm^{-1} as shown in Fig. 13, which were correlated to the oxygen vacancies generated as charge compensating defect [32], which is more beneficial to the migration of oxide-ionic.

4. Conclusions

Powders $Ce_{0.9}Sr_{0.1}Cr_{0.5}Fe_{0.5}O_{3-\delta}$ prepared by gel combustion method are suitable as anode for H_2S/air SOFC. The highest conductivities of catalysts measured are 2.37 S cm^{-1} in 3% H_2–N_2 and 2.92 S cm^{-1} in H_2S at 800 °C, respectively. CSCrF materials exhibit good chemical compatibility with SDC in N_2. For the cell comprising of CSCrF–SDC/SDC/Ag, the maximum open circuit voltage is 0.86 V and the maximum power density is 18.75 mW cm^{-2} in 5% H_2S–N_2 at 600 °C. The max OCV is 0.95 V and the max power density is 13.1 mW cm^{-2} in 3% H_2–N_2 at 500 °C. From the analysis of EIS and the equivalent circuit, at low temperature, polarization resistance is the main reason affecting the performance of the cell. The area specific resistance significantly decreases with the increasing temperature. After cell test, the Roman of electrolyte SDC is analyzed and gets a conclusion that SDC has not been reacted with H_2 at 500 °C.

Acknowledgments

The work was supported by the Funds of Nature Science of Jiangsu Province (Grant Nos. BF2006208 and BK2010478).

References

[1] N. Danilovic, J.L. Luo, K.T. Chuang, A.R. Sanger, J. Power Sources 194 (2009) 252–262.
[2] N. Danilovic, J.L. Luo, K.T. Chuang, A.R. Sanger, J. Power Sources 192 (2009) 247–257.
[3] V. Vorontsov, J.L. Luo, A.R. Sanger, K.T. Chuang, J. Power Sources 183 (2008) 76–83.
[4] J. Ober, US Geol. Surv. 74 (2004) 1–18.
[5] D.K. Beavon, B. Kouzel, J.W. Ward, Chem. Am. Chem. Soc. 26 (1981) 237–245.
[6] L.J. Song, G.W. Du, Y. Di, Chem. Ind. For. Prod. 19 (1999) 1–8.
[7] N.U. Pujare, K.W. Semkow, A.F. Sammells, J. Electrochem. Soc. 134 (1987) 2639–2640.
[8] A.F. Sammells, J. Patel, J. Osborne, R.L. Cook, Gas Sep. Purif. 6 (1992) 141–147.
[9] T.J. Kirk, J. Winnick, J. Electrochem. Soc. 140 (1993) 3494–3496.
[10] B.G. Ong, T.A. Lin, D.M. Mason, Proc. Electrochem. Soc. Ser. 12 (1987) 295–306.
[11] D. Weaver, J. Winnick, J. Electrochem. Soc. 134 (1987) 2451–2458.
[12] Z. Xu, J. Luo, K.T. Chuang, J. Electrochem. Soc. 154 (2007) B523–B527.
[13] N.M. Galea, E.S. Kadantsev, T. Ziegler, J. Phys. Chem. C 113 (2009) 193–203.
[14] D. Peterson, J. Winnick, J. Electrochem. Soc. 145 (1998) 1449–1453.
[15] M. Liu, P. He, G. Wei, J. Luo, A.R. Sanger, K.T. Chuang, J. Power Sources 94 (2001) 20–25.
[16] C. Yates, J. Winnick, J. Electrochem. Soc. 146 (1999) 2841–2844.
[17] M.S. Miao, H.X. Qu, Q. Zhong, W.Y. Tan, New Chem. Mater. 36 (2008) 70–75 (in Chinese).
[18] F. Feng, H.X. Qu, W.Y. Tan, Q. Zhong, Chin. J. Appl. Chem. 25 (2008) 199–203 (in Chinese).
[19] L. Aguilar, S. Zha, Z. Cheng, J. Winnick, M. Liu, J. Power Sources 135 (2004) 17–24.
[20] L. Aguilar, S. Zha, S. Li, J. Winnick, M. Liu, Electrochem. Solid-State Lett. 7 (2004) A324–A326.
[21] Z. Cheng, S. Zha, L. Aguilar, D. Wang, J. Winnick, M. Liu, Mixtures Electrochem. Solid-State Lett. 9 (2006) A31–A33.
[22] S. Hui, A. Petric, Solid State Ionics 143 (2001) 275–283.
[23] Z. Cheng, S. Zha, L. Aguilar, M. Liu, Solid State Ionics 176 (2005) 1921–1928.
[24] C. Reiichi, Y. Bunichi, S. Yoji, T. Yoshitaka, A. Masayasu, Japanese Patent, JP2004186148A.
[25] W.C. Wu, J.T. Huang, A. Chiba, J. Power Sources 195 (2010) 5868–5874.
[26] X.F. Zhu, Q. Zhong, X.J. Zhao, H. Yan, Appl. Surf. Sci. 257 (2011) 1967–1971.
[27] C. Kittel, Introduction to Solid State Physics, 8th ed., Wiley, Berkley, CA, 2005.
[28] Y.F. Zheng, M. Zhou, L. Ge, S.J. Li, H. Chen, L.C. Guo, J. Alloys Compd. 509 (2011) 1244–1248.
[29] F.H. Heuveln, H.J.M. Bouwmeester, J. Electrochem. Soc. 144 (1997) 134–140.
[30] Y.J. Leng, S.H. Chan, K.A. Khor, S.P. Jiang, Int. J. Hydrogen Energy 29 (2004) 1025–1033.
[31] S.Q. Lv, G.H. Long, Y. Ji, X.W. Meng, H.Y. Zhao, C.C. Sun, J. Alloys Compd. 509 (2011) 2824–2828.
[32] J.R. McBride, K.C. Hass, B.D. Poindexter, W.H. Weber, J. Appl. Phys. 76 (1994) 2435–2441.
[33] M. Zunica, L. Chevallier, A. Radojkovic, G. Brankovic, Z. Brankovic, E.D. Bartolomeo, J. Alloys Compd. 509 (2011) 1157–1162.
[34] J.M. Im, H.J. You, Y.S. Yoon, D.W. Shin, Ceram. Int. 34 (2008) 877–881.
[35] E.C.C. Souza, E.N.S. Muccillo, J. Alloys Compd. 473 (2009) 560–566.